


## Nanostructured pumped-corner state in a kagome lattice

A. Jazmín Tapia-de-la-Rosa<sup>✉\*</sup> and J. Eduardo Barrios-Vargas<sup>✉†</sup>

*Departamento de Física y Química Teórica, Facultad de Química, Universidad Nacional Autónoma de México, Ciudad de México 04510, Mexico*

 (Received 11 September 2023; revised 8 December 2023; accepted 16 January 2024; published 2 February 2024)

Bulk-boundary correspondence establishes the connection between the topological properties of the bulk and the edge states when a boundary is present. However, the boundary can be tailored to tune the appearance of the edge states. Using a higher-order topological Hamiltonian, we engineered the appearance of a one-corner state that can be translated between corners with a periodic parameter. As a result, we established that this is a pumping mechanism. The one-corner state is characterized using the inverse participation ratio, and we establish that the state has a topological invariant associated. Consequently, the state is topologically protected. Finally, we explore the robustness to random disorder.

DOI: [10.1103/PhysRevB.109.085402](https://doi.org/10.1103/PhysRevB.109.085402)

### I. INTRODUCTION

Topological matter has emerged as a notable research area in condensed matter physics. One consequence of the topology is the appearance of edge states at the boundaries, known as the bulk-boundary correspondence [1–7]. A possible classification of topological matter is using the dimension of the topological edge states compared to the dimension of the boundary; this classification leads to higher-order topological matter [8–10]. Currently, phononic, photonic, and electrical circuits have been utilized to achieve the experimental realization of higher-order topological insulators (HOTIs) [11–14] and higher-order topological semimetals (HOTSMs) [15–17].

The layout of the nanosystem's boundaries will be intricately linked to the symmetries of the entire crystal. The theoretical rise of the corner and hinge states in terms of the symmetries of the higher-order topological crystals has been explained previously in terms of the *filling anomaly*, which plays a crucial role in understanding the emergence of these lower-dimensional topological boundary states [18,19]. Typically, the physical properties at the nanoscale strongly depend on the boundary. However, there is a trade-off between the topological and trivial edge states in the topological matter. Especially, the extension of the edge states of a higher-order topological matter (HOTM) can depend on the shape of the boundary [20–22].

In this paper, we explore a three-dimensional (3D) second-order topological Hamiltonian, a three-dimensional system exhibiting topological edge states in 1D, commonly called hinge states [23]. Analogously, a two-dimensional system would be a 2D second-order topological material, which will possess topological states in 0D, better known as corner states. As in conventional topological materials, these corner or hinge states will be robust against perturbations and impurities, which means that even in the presence of disorder,

these states will persist. Such robustness makes higher-order topological matter attractive for potential applications in electronics [24,25] and quantum computing [26]. We focus on one of the most intriguing phenomena of HOTMs, known as *adiabatic pumping* or Thouless pumping [27]. Topological pumping in HOTMs is characterized by topological states (pumping states) that traverse bulk states and transport states from one corner of a structure to the opposite corner by periodically and adiabatically evolving their Hamiltonian over time. Recent experiments have successfully demonstrated the existence of pumping states in photonic crystals [28] using a Hamiltonian with  $C_6$  symmetry. In contrast, we investigate the pumping behavior of one corner state in a  $C_3$  symmetric higher-order topological Hamiltonian using a tight-binding model approach of the kagome lattice [29]. Our research demonstrates that the edge states of this crystal can exhibit pumping between two corner states only when the nanosystem's geometry takes on the specific form of a parallelogram. This phenomenon is achieved by introducing a temporal dependence into the three-dimensional equivalence of its Hamiltonian. In the following, we present the tight-binding Hamiltonian for the three-dimensional lattice and employ the above-mentioned approaches to propose a time-dependent Hamiltonian capable of pumping the corner states and also analyze their robustness against perturbations.

### II. MODEL

We introduce the tight-binding model for our tridimensional system, comprising bidimensional stacked layers composed of a kagome lattice with the lattice vectors of the unit cell  $\mathbf{a}_1 = a(1, 0, 0)$ ,  $\mathbf{a}_2 = a(1/2, \sqrt{3}/2, 0)$ , and  $\mathbf{a}_3 = h(0, 0, 1)$ . Within each layer, three sites, denoted as A, B, and C per unit cell, are interconnected by intracell hoppings denoted as  $t_{\text{intra}}$ . Furthermore, intercell hopping  $t_{\text{inter}}$  establishes connections between each unit cell, while diagonal hoppings  $t_z$  couple the bidimensional layers. The model's geometry is illustrated in Fig. 1, and the bulk spinless Hamiltonian of the

\*jazmintapia@ciencias.unam.mx

†j.e.barrios@gmail.com

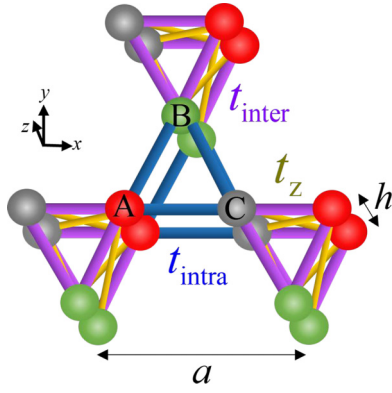


FIG. 1. Schematic of the crystal structure. With intracell hopping  $t_{\text{intra}}$ , intercell hopping  $t_{\text{inter}}$ , and interlayer hopping  $t_z$ ;  $a$  and  $h$  represent lattice constants in the  $x$ - $y$  plane and  $z$  direction, respectively.

system is given by [23,30]

$$H(\mathbf{k}) = \begin{bmatrix} 0 & h_{AB} & h_{AC} \\ h_{AB}^* & 0 & h_{BC} \\ h_{AC}^* & h_{BC}^* & 0 \end{bmatrix}, \quad (1)$$

where  $h_{AB} = t_{\text{intra}} + t'_{\text{inter}} e^{-i(\mathbf{k} \cdot \mathbf{a}_2)}$ ,  $h_{AC} = t_{\text{intra}} + t'_{\text{inter}} e^{-i(\mathbf{k} \cdot \mathbf{a}_1)}$ , and  $h_{BC} = t_{\text{intra}} + t'_{\text{inter}} e^{i[\mathbf{k} \cdot (\mathbf{a}_2 - \mathbf{a}_1)]}$ , where  $t'_{\text{inter}} = t_{\text{inter}} + 2t_z \cos(k_z h)$ . Particularly, the breathing kagome lattice has demonstrated performing as both a HOTI [31–34] and a HOTSM [30]. In accordance with Ref. [30],

in the semimetal case  $t_{\text{intra}} = t'_{\text{inter}}$  and the degenerate points correspond to  $\mathbf{K}_{\pm} = (4\pi/3a, 0, \pm k_w/h)$ , where  $k_w = \arccos(t_{\text{intra}} - t_{\text{inter}}/2t_z)$ . The bulk Hamiltonian can also be written in the form

$$H(\mathbf{k}) = t_{\text{intra}} \hat{h}_{\text{intra}} + [t_{\text{inter}} + t_z \cos(k_z/h)] \hat{h}_{\text{inter}}(k_x, k_y), \quad (2)$$

where

$$\hat{h}_{\text{intra}} = \begin{bmatrix} 0 & 1 & 1 \\ 1 & 0 & 1 \\ 1 & 1 & 0 \end{bmatrix},$$

$$\hat{h}_{\text{inter}}(k_x, k_y) = \begin{bmatrix} 0 & e^{-ia_2 \cdot \mathbf{k}} & e^{-ia_1 \cdot \mathbf{k}} \\ e^{ia_2 \cdot \mathbf{k}} & 0 & e^{i(a_2 - a_1) \cdot \mathbf{k}} \\ e^{ia_1 \cdot \mathbf{k}} & e^{-i(a_2 - a_1) \cdot \mathbf{k}} & 0 \end{bmatrix}. \quad (3)$$

### A. Parallelogram geometry

We aimed to model nanostructures capable of exhibiting higher-order topological states. Previously, in the particular case when the nanosystem takes on a triangular geometry, it has been shown that the topological edge states can be localized at the corner or bearded edge in the lattice [20,33]. Figure 2 illustrates three systems' structures and energy bands with parallelogram geometry in the  $x$ - $y$  plane. While these systems share the same global geometry, slight variations in

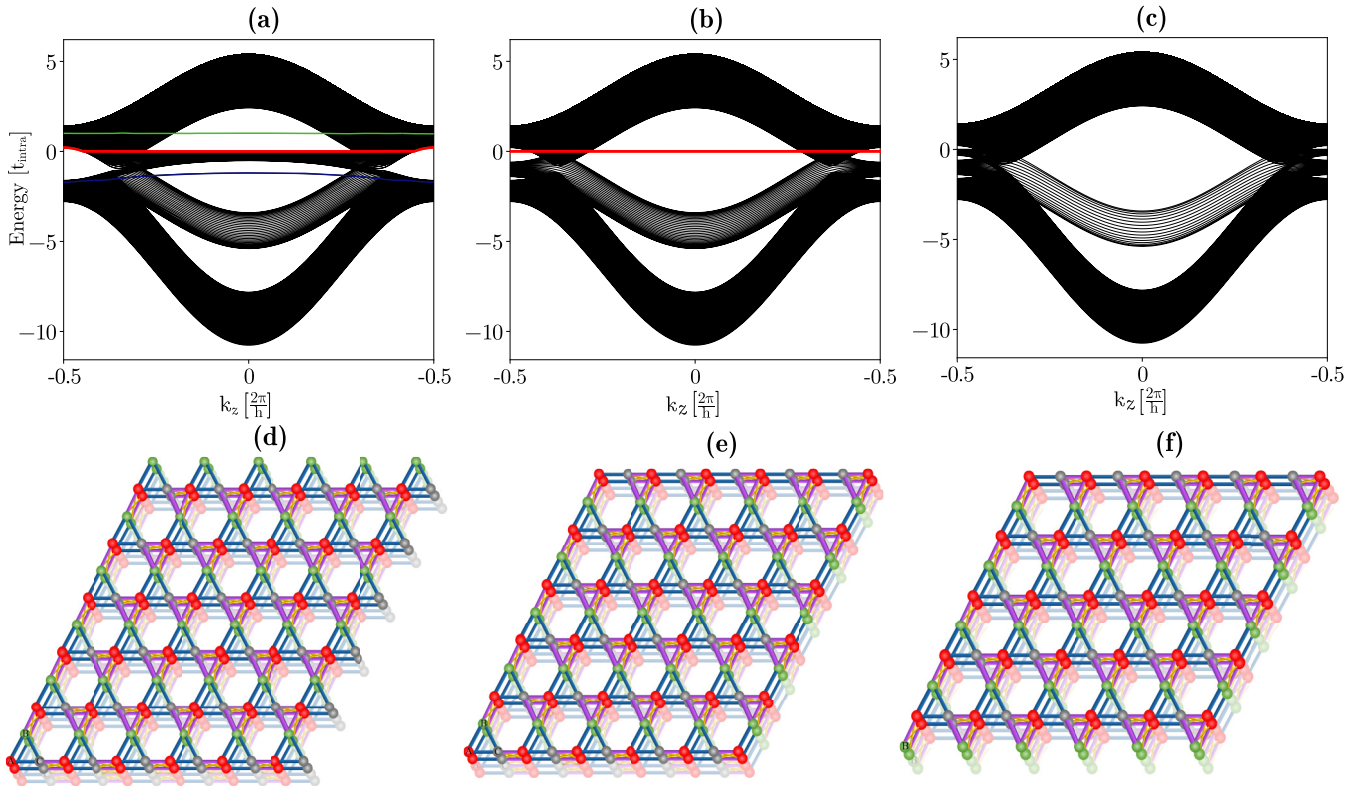


FIG. 2. Energy spectra of three types of parallelogram systems. The dispersion bands [(a)–(c)] correspond to the geometries [(d)–(f)], respectively. The parameters for all cases were chosen as  $t_{\text{intra}} = -1$ ,  $t_{\text{inter}} = -2.4$ , and  $t_z = -1$  in arbitrary units. The lattice constants  $a$  and  $h$  are chosen as unity. To calculate the dispersion bands in [(a)–(c)], we considered  $L = 17$  unit cells along the  $x$ - $y$  edges of the parallelogram.

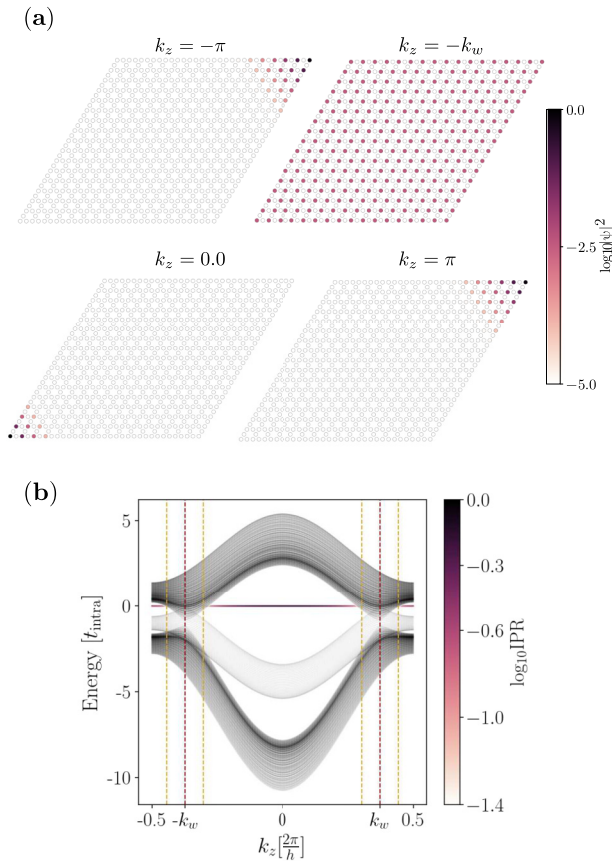


FIG. 3. Zero-energy pumped state. (a) Probability density of states for four representative  $k_z$  values of the zero-energy state for the geometry in Fig. 2(e). (b) Band structure colored by IPR for the case shown in Fig. 2(b). The dotted lines indicate the areas where the zero-energy flat band overlaps with the bulk bands. The lattice parameters for all cases are the same as in Fig. 2. We considered  $L = 17$  unit cells along the  $x$ - $y$  edges of the parallelogram.

the boundary geometry lead to distinct appearances of zero-energy states.

In the first case [Fig. 2(a)], we observe two zero-energy boundary states and two boundary states with energies  $E = \pm 1[t_{\text{intra}}]$ . The second case [Fig. 2(b)] arises from the first case by cutting the sites at their top and right boundaries, resulting in one zero-energy state. In contrast, the third case emerges from cutting the bottom of the second case, and in this geometry, we do not obtain states with zero energy [Fig. 2(c)]. These examples highlight the relevance of the system's edge geometry and the robustness of its energy bands to changes in geometry.

We focus on the case illustrated in Fig. 2(b). To investigate the emergence of corner states for this system, we present the top view of the probability density for the zero-energy flat band in Fig. 3(a), varying the parameter  $k_z$ . At  $k_z = \pm\pi$ , the flat band localizes at the upper right corner of the parallelogram, while at  $k_z = 0$ , the state localizes at the lower left corner. The state delocalizes along the system for  $k_z \sim \pm k_w$ . To visualize the degree of localization of the zero-energy state, we plot the energy bands in Fig. 3(b) for this geometry depending on the value of the inverse participation ratio (IPR)

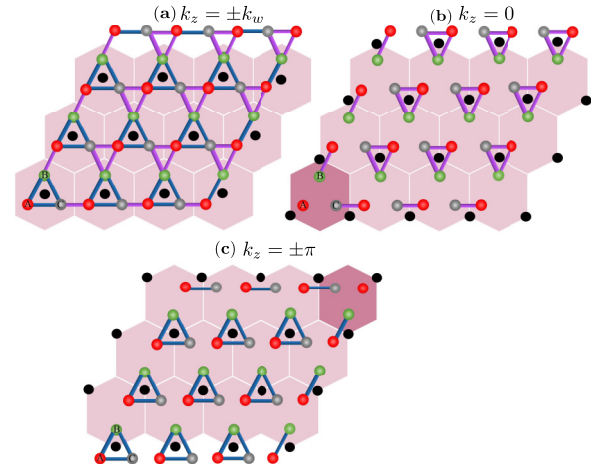


FIG. 4. Schematic representation of Wannier centers in the trivial and topological phases protected by  $C_3$  symmetry. (a) represents the trivial topological phase. The red, green, and gray sites are the sites of the kagome lattice, while the black dots represent the Wannier centers. (b) and (c) represent the OAL topological phases where we have a filling anomaly. The pink hexagons delimit the unit cells.

[35,36]. The most localized state corresponds to the flat band with zero energy. This observation suggests the possibility of a higher-order topological charge pumping from the upper right corner to the lower left corner using the  $k_z$  parameter.

## B. Topological protection

Following Ref. [30], the second-order topological index ensures the localization of corner or hinge states and their quantization and protection by the crystalline symmetries of the system. These symmetries also govern the positions of Wannier centers, aligning them with the maximal Wyckoff positions in the unit cell [9,28]. For the system proposed in this study, the  $C_3$  symmetry protects the second-order topological index [37], resulting in Wannier centers at the corners of the unit cells [23]. As we will show below, this leads to a quantized charge at either the upper right or upper left corner of the parallelogram system; this phenomenon is better known as a *filling anomaly* [18,19]. In contrast, the trivial phase is characterized by Wannier centers positioned at the centers of the unit cells, without any filling anomaly [black dots in Fig. 4(a)].

Consequently, the proposed charge pumping adiabatically connects the trivial and nontrivial phases [commonly known as obstructed atomic limit (OAL) phases] through the parameter  $k_z$ . An intuitive way to illustrate how the concentration of a state at a corner occurs in these crystalline systems is by visualizing them as extensions of the Su-Schrieffer-Heeger (SSH) model. In Fig. 4(b), the OAL corresponding to  $t_{\text{intra}} = 0$  is illustrated where the black dots represent the Wannier centers. In this limit, it becomes evident that the bottom-left boundary is separated completely from the bulk, and that corner corresponds to an isolated site of two dimerized chains of the SSH model. It is crucial to emphasize that both chains share a single isolated site, resulting in a zero-energy state.

The other OAL phase is illustrated in Fig. 4(c), where  $t_{\text{inter}} = 0$ . In this limit, the two dimerized chains of the SSH



TABLE I. Topological invariant indices for  $C_3$  symmetry generators. According to Ref. [18],  $h_{2c}^{(3)}$  and  $h_{2b}^{(3)}$  represent the primitive generators of the rotation symmetry and their corresponding topological invariants.

Symmetry	Generator	Invariants	
		$[\mathbf{K}_1^{(3)}]$	$[\mathbf{K}_2^{(3)}]$
$C_3$	$h_{2c}^{(3)}$	1	0
	$h_{2b}^{(3)}$	1	-1

model allow one isolated site at the top-right boundary of the parallelogram. As a result, the system hosts a zero-energy state. This state represents a topological state protected by the system's crystalline symmetries and the invariant associated with its generator,  $h_{2c}^{(3)}$  [18].

Moreover, we will delve into the topological invariants arising from the crystal symmetries of our system, following the approach proposed by Benalcazar *et al.* [18,28] which was addressed before in Ref. [38] considering symmetry reps to form invariants generally. Because our model includes two OAL phases protected by  $C_3$  symmetry, their topological classification is determined by the following indices [18],

$$\chi^{(3)} = ([\mathbf{K}_1^{(3)}], [\mathbf{K}_2^{(3)}]), \quad (4)$$

where  $[\mathbf{K}_1^{(3)}]$  and  $[\mathbf{K}_2^{(3)}]$  are the integer topological invariants which can be calculated through the values established in Table I [18].

The topological invariant  $\chi^{(3)}$  holds a direct connection to primitive generators of the crystalline system denoted as  $h_{m\text{Center}}^{(n)}$  where  $m$  denoted the filled bands with the Wannier centers at the center position for a  $C_n$  rotation symmetry [18], providing a physical understanding of the filling anomaly emergence. These system generators may vary depending on the positions of their Wannier centers, which are fixed based on the maximal Wyckoff positions of the unit cell. When  $k_z = \pm\pi$ , our tight-binding Hamiltonian exhibits a corresponding primitive generator known as  $h_{2c}^{(3)}$  [18]. This generator localizes three Wannier centers: two at the upper corners and one at the lower corner of the hexagonal unit cell [black dots in Fig. 4(c)].

Upon analyzing the positions of the Wannier centers at the boundaries in the parallelogram-shaped system shown in Fig. 4(c) (black dots), a discrepancy between the number of unit cells and the number of Wannier centers on the right and upper boundaries becomes clear. This discrepancy leads to a filling anomaly, resulting in a nonzero polarization and the localization of a state in the upper-right corner, which correlates with the probability density of the flat band illustrated in Fig. 3(a). As a consequence, the topological index indicates a nontrivial phase (OAL phase), and, based on Table I, it takes the value  $\chi^{(3)} = (1, 0)$ .

Similarly, at  $k_z = 0$ , the corresponding primitive generator is denoted as  $h_{2b}^{(3)}$ , leading to a topological index value of  $\chi^{(3)} = (1, -1)$ . In this case, the Wannier centers are located at one upper corner and two lower corners of the unit cells [black dots in Fig. 4(b)]. Upon analyzing the figure, it becomes evident that there is a mismatch between the number of unit cells

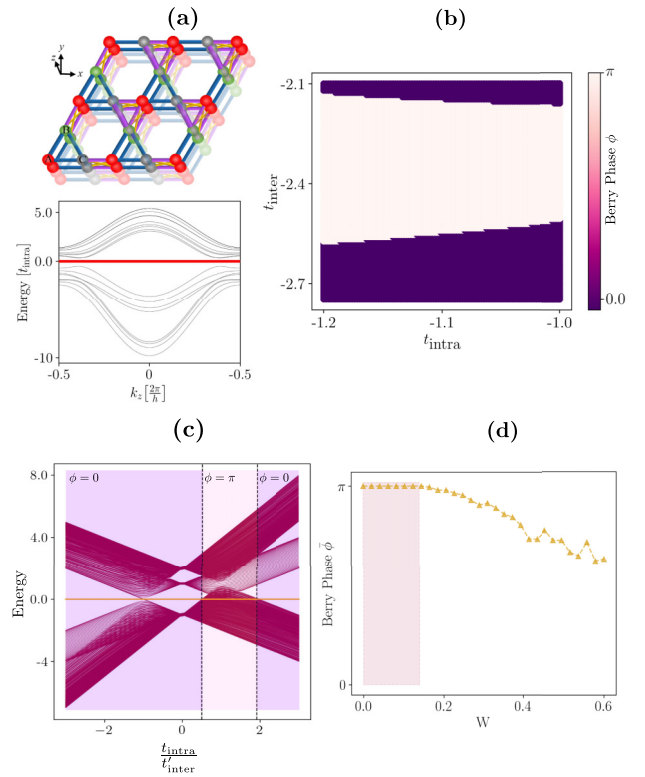


FIG. 5. Multiband Berry phase. (a) Geometry of the system and energy spectrum for the calculus of the multiband Berry phase in (b) and (d) with  $L = 3$  unit cells along the  $x$ - $y$  edges, (b) multiband Berry phase depending of the value of the hoppings  $t_{\text{intra}}$  and  $t_{\text{inter}}$ , (c) energy spectrum depending of the ratio  $t_{\text{intra}}/t_{\text{inter}}$  using  $L = 20$  unit cells along the  $x$ - $y$  edges of the parallelogram, and (d) average multiband phase vs Anderson-type disorder parameter  $W$ . The values of the parameters  $t_{\text{intra}}$ ,  $t_{\text{inter}}$ , and  $t_z$  for this case are the same as in Fig. 2.

and the number of the Wannier centers on the bottom and left boundaries of the parallelogram. As a result, a filling anomaly occurs again, leading to nonzero polarization and state localization in the bottom-left corner [see Fig. 3(a)]. Notice that the model is protected by  $C_3$  but the edge configuration clearly breaks  $C_3$ . However, the positions of the Wannier centers remain unchanged for the corresponding hexagonal unit cells on the edge, despite the breaking of  $C_3$ . When  $k_z = \pm k_w$ , the topological index takes the trivial value of  $\chi^{(3)} = (0, 0)$ . In these cases, there is no filling anomaly as the Wannier centers are positioned at the centers of the unit cells [black dots in Fig. 4(a)], leading to a delocalization of the state along the system.

### C. Robustness to disorder

In Fig. 5(a) we present the special case of the parallelogram geometry with  $L = 3$  unit cells along the  $x$ - $y$  edges and their energy bands where the zero-energy flat band is isolated from the other bands. Therefore, the bands for this system size do not present degeneracy, and we can calculate the multiband Berry phase without considering degeneracy [39]. For this system, Fig. 5(b) displays the multiband Berry phase of the bands less than and equal to zero as a function of the values of

the couplings  $t_{\text{intra}}$  and  $t_{\text{inter}}$ . In this graph, we can identify the case portrayed in Fig. 3, where  $t_{\text{intra}} = -1.0$  and  $t_{\text{inter}} = -2.4$  exhibiting a multiband phase equal to  $\pi$ , and a range of values where the multiband phase is equal to  $\pi$ . This means the presence of a pumping state. Inducing a phase in this type of pumping arises from the shift in the positions of the Wannier centers. The transition region without a multiband phase (and hence the loss of pumping state) in Fig. 5(b) is consistent with the energy bands of  $L = 20$  unit cells along the  $x$ - $y$  edges of the parallelogram plotted in Fig. 5(c). In Fig. 5(c), the region outside the vertical dashed lines is recognized where the flat band with energy  $E = 0$  does not have contact with the bulk bands, consequently leading to the absence of pumping.

We also examined the robustness of the topological states in the presence of Anderson-type disorder, which involves varying the on-site energies within a range of uniform random values between  $-W$  and  $W$ , where  $W$  is a disorder parameter. Previous studies have demonstrated that disorder can induce a transition of the topological Thouless pumping to a trivial phase. However, it has also been found that the topological pumping will persist under weak disorder [40]. In Fig. 5(d), we present the average multiband phase value as a function of the disorder strength  $W$ . It is evident that as  $W$  increases, the average multiband phase deviates from its  $\pi$  value and starts to decrease. The region where the average multiband phase remains relatively constant [depicted as the light red zone in Fig. 5(d)] allows us to identify the range of robustness of the topological pumping against Anderson-type disorder.

### III. EXPERIMENTAL REALIZATION

According to Fig. 3, the transport from one corner to another is possible through the eigenstate corresponding to the flat band in Fig. 3(b) if we take the parameter  $k_z$  and change it to a temporal parameter. The time-dependent Hamiltonian for the kagome crystalline system, in this case, changes to  $\mathcal{H}(t) = t_{\text{intra}}\hat{h}_{\text{intra}} + t_{\text{inter}}\hat{h}_{\text{inter}} + H(t)$ , where  $H(t) = 2t_z \cos(t/T)\hat{h}_{\text{inter}}$ . The terms  $\hat{h}_{\text{inter}}$  and  $\hat{h}_{\text{intra}}$  correspond to (3). In the published work by Benalcazar *et al.* [28], they present a novel realization

of a higher-order pumping state using photonic waveguides. The essence of this pumping technique revolves around extending a 3D crystalline system into a 2D system with an additional temporal coordinate. The pumping process is accomplished through the adiabatic modulation of a specific parameter in the Hamiltonian. Consequently, the system proposed in this study suggests the possibility of its realization in a similar manner. Another proposed experimental alternative is through acoustic crystals, where zero-energy corner topological states have previously been observed in Ref. [41]. Yet another alternative could be topoelectrical circuits, which have also demonstrated the experimental realization of corner modes [42]. A 2D acoustic crystal with a parallelogram geometric shape has previously been experimentally realized in Ref. [33], where a corner state was observed. Recently, corner state transfer mapping has been experimentally carried out using acoustic crystals [43].

### IV. CONCLUSION

Ultimately, the findings of this study demonstrate that although the geometry of the nanosystem does not maintain the identical symmetry of the crystalline unit cell from which it emerges, a bulk-boundary correspondence persists. We provide an intuitive approach to anticipate the emergence of corner states within a nanosystem at  $E = 0$ , and we identify the need for the zero-energy state mix with the bulk states to have a corner-to-corner pumping mechanism. Conversely, we introduce a time-dependent Hamiltonian with the potential to control these states and facilitate charge pumping from one corner to another. Such a phenomenon holds promise for practical implementation within photonic crystals through experimentation.

### ACKNOWLEDGMENTS

A.J.T.R. gratefully acknowledges support via a CONAHCYT graduate scholarship. We gratefully acknowledge funding from CONAHCYT Proyecto Frontera 428214, UNAM-DGAPA (project Grant No. PAPIIT IA106021).

- 
- [1] Y. Hatsugai, Chern number and edge states in the integer quantum Hall effect, *Phys. Rev. Lett.* **71**, 3697 (1993).
  - [2] M. Z. Hasan and C. L. Kane, *Colloquium: Topological insulators*, *Rev. Mod. Phys.* **82**, 3045 (2010).
  - [3] J. E. Moore, The birth of topological insulators, *Nature (London)* **464**, 194 (2010).
  - [4] J. Cayssol and J. N. Fuchs, Topological and geometrical aspects of band theory, *J. Phys.: Mater.* **4**, 034007 (2021).
  - [5] X.-L. Qi and S.-C. Zhang, Topological insulators and superconductors, *Rev. Mod. Phys.* **83**, 1057 (2011).
  - [6] G. M. Graf and M. Porta, Bulk-edge correspondence for two-dimensional topological insulators, *Commun. Math. Phys.* **324**, 851 (2013).
  - [7] J.-W. Rhim, J. H. Bardarson, and R.-J. Slager, Unified bulk-boundary correspondence for band insulators, *Phys. Rev. B* **97**, 115143 (2018).
  - [8] W. A. Benalcazar, B. A. Bernevig, and T. L. Hughes, Quantized electric multipole insulators, *Science* **357**, 61 (2017).
  - [9] W. A. Benalcazar, B. A. Bernevig, and T. L. Hughes, Electric multipole moments, topological multipole moment pumping, and chiral hinge states in crystalline insulators, *Phys. Rev. B* **96**, 245115 (2017).
  - [10] B. Xie, H.-X. Wang, X. Zhang, P. Zhan, J.-H. Jiang, M. Lu, and Y. Chen, Higher-order band topology, *Nat. Rev. Phys.* **3**, 520 (2021).
  - [11] C. W. Peterson, W. A. Benalcazar, T. L. Hughes, and G. Bahl, A quantized microwave quadrupole insulator with topologically protected corner states, *Nature (London)* **555**, 346 (2018).
  - [12] M. Serra-Garcia, V. Peri, R. Süsstrunk, O. R. Bilal, T. Larsen, L. G. Villanueva, and S. D. Huber, Observation of a phononic quadrupole topological insulator, *Nature (London)* **555**, 342 (2018).
  - [13] B.-Y. Xie, H.-F. Wang, H.-X. Wang, X.-Y. Zhu, J.-H. Jiang, M.-H. Lu, and Y.-F. Chen, Second-order photonic topological insulator with corner states, *Phys. Rev. B* **98**, 205147 (2018).

- [14] J. Noh, W. A. Benalcazar, S. Huang, M. J. Collins, K. P. Chen, T. L. Hughes, and M. C. Rechtsman, Topological protection of photonic mid-gap defect modes, *Nat. Photon.* **12**, 408 (2018).
- [15] L. Luo, H.-X. Wang, Z.-K. Lin, B. Jiang, Y. Wu, F. Li, and J.-H. Jiang, Observation of a phononic higher-order Weyl semimetal, *Nat. Mater.* **20**, 794 (2021).
- [16] H. Qiu, M. Xiao, F. Zhang, and C. Qiu, Higher-order Dirac sonic crystals, *Phys. Rev. Lett.* **127**, 146601 (2021).
- [17] C.-H. Xia, H.-S. Lai, X.-C. Sun, C. He, and Y.-F. Chen, Experimental demonstration of bulk-hinge correspondence in a three-dimensional topological dirac acoustic crystal, *Phys. Rev. Lett.* **128**, 115701 (2022).
- [18] W. A. Benalcazar, T. Li, and T. L. Hughes, Quantization of fractional corner charge in  $C_n$ -symmetric higher-order topological crystalline insulators, *Phys. Rev. B* **99**, 245151 (2019).
- [19] Y. Fang and J. Cano, Filling anomaly for general two- and three-dimensional  $C_4$  symmetric lattices, *Phys. Rev. B* **103**, 165109 (2021).
- [20] F. K. Kunst, G. van Miert, and E. J. Bergholtz, Lattice models with exactly solvable topological hinge and corner states, *Phys. Rev. B* **97**, 241405(R) (2018).
- [21] R. Queiroz and A. Stern, Splitting the hinge mode of higher-order topological insulators, *Phys. Rev. Lett.* **123**, 036802 (2019).
- [22] R. Queiroz, I. C. Fulga, N. Avraham, H. Beidenkopf, and J. Cano, Partial lattice defects in higher-order topological insulators, *Phys. Rev. Lett.* **123**, 266802 (2019).
- [23] M. Ezawa, Higher-order topological insulators and semimetals on the breathing kagome and pyrochlore lattices, *Phys. Rev. Lett.* **120**, 026801 (2018).
- [24] A.-Q. Wang, X.-G. Ye, D.-P. Yu, and Z.-M. Liao, Topological semimetal nanostructures: From properties to topotronics, *ACS Nano* **14**, 3755 (2020).
- [25] L. Song, H. Yang, Y. Cao, and P. Yan, Square-root higher-order Weyl semimetals, *Nat. Commun.* **13**, 5601 (2022).
- [26] Y. You, D. Litinski, and F. von Oppen, Higher-order topological superconductors as generators of quantum codes, *Phys. Rev. B* **100**, 054513 (2019).
- [27] D. J. Thouless, Quantization of particle transport, *Phys. Rev. B* **27**, 6083 (1983).
- [28] W. A. Benalcazar, J. Noh, M. Wang, S. Huang, K. P. Chen, and M. C. Rechtsman, Higher-order topological pumping and its observation in photonic lattices, *Phys. Rev. B* **105**, 195129 (2022).
- [29] H.-M. Guo and M. Franz, Topological insulator on the kagome lattice, *Phys. Rev. B* **80**, 113102 (2009).
- [30] Q. Wei, X. Zhang, W. Deng, J. Lu, X. Huang, M. Yan, G. Chen, Z. Liu, and S. Jia, Higher-order topological semimetal in acoustic crystals, *Nat. Mater.* **20**, 812 (2021).
- [31] X. Ni, M. A. Gorlach, A. Alu, and A. B. Khanikaev, Topological edge states in acoustic kagome lattices, *New J. Phys.* **19**, 055002 (2017).
- [32] M. Ezawa, Higher-order topological electric circuits and topological corner resonance on the breathing kagome and pyrochlore lattices, *Phys. Rev. B* **98**, 201402(R) (2018).
- [33] H. Xue, Y. Yang, F. Gao, Y. Chong, and B. Zhang, Acoustic higher-order topological insulator on a kagome lattice, *Nat. Mater.* **18**, 108 (2019).
- [34] H.-X. Wang, L. Liang, B. Jiang, J. Hu, X. Lu, and J.-H. Jiang, Higher-order topological phases in tunable  $C_3$  symmetric photonic crystals, *Photonics Res.* **9**, 1854 (2021).
- [35] J. T. Edwards and D. J. Thouless, Numerical studies of localization in disordered systems, *J. Phys. C: Solid State Phys.* **5**, 807 (1972).
- [36] M. Calixto and E. Romera, Inverse participation ratio and localization in topological insulator phase transitions, *J. Stat. Mech.: Theory Exp.* (2015) P06029.
- [37] The Hamiltonian model is spinless with symmetry class AI of the tenfold classification with zero on-site energies.
- [38] J. Kruthoff, J. de Boer, J. van Wezel, C. L. Kane, and R.-J. Slager, Topological classification of crystalline insulators through band structure combinatorics, *Phys. Rev. X* **7**, 041069 (2017).
- [39] To calculate the multiband Berry phase, we employ the expression  $\phi = \sum_{n=1}^{\text{occ}} -\text{Im} \ln[\langle u_{n,0} | u_{n,1} \rangle \langle u_{n,1} | u_{n,2} \rangle \cdots \langle u_{n,N} | u_{n,0} \rangle]$ , where occ corresponds to the band index of the zero-energy band,  $|u_{n,i}\rangle$  is the eigenvector of the  $n$  band for  $k_z = (i/N)\pi$ , and  $N = 400$ . Note that values of  $k_z$  correspond to a path within the irreducible Brillouin zone.
- [40] C. Lu, Z.-F. Cai, M. Zhang, H. Wang, Q. Ai, and T. Liu, Effects of disorder on Thouless pumping in higher-order topological insulators, *Phys. Rev. B* **107**, 165403 (2023).
- [41] Y. Deng, W. A. Benalcazar, Z.-G. Chen, M. Oudich, G. Ma, and Y. Jing, Observation of degenerate zero-energy topological states at disclinations in an acoustic lattice, *Phys. Rev. Lett.* **128**, 174301 (2022).
- [42] S. Imhof, C. Berger, F. Bayer, J. Brehm, L. W. Molenkamp, T. Kiessling, F. Schindler, C. H. Lee, M. Greiter, T. Neupert, and R. Thomale, Topoelectrical-circuit realization of topological corner modes, *Nat. Phys.* **14**, 925 (2018).
- [43] H. Liu, H. Wang, B. Xie, H. Cheng, Z. Liu, and S. Chen, Acoustic corner state transfer mapping to synthetic higher-order topological semimetal, *Phys. Rev. B* **108**, L161104 (2023).